

# The Cluster AgeS Experiment (CASE).<sup>†</sup> Variable stars in the field of the globular cluster M10<sup>\*</sup>

M. R o z y c z k a<sup>1</sup>, W. N a r l o c h<sup>1,2,3</sup>,  
A. S c h w a r z e n b e r g – C z e r n y<sup>1</sup>,  
I. B. T h o m p s o n<sup>4</sup> R. P o l e s k i<sup>5</sup> and W. P y c h<sup>1</sup>,

<sup>1</sup>Nicolaus Copernicus Astronomical Center, ul. Bartycka 18, 00–716 Warsaw,  
Poland

e-mail: (mnr, wnarloch, psych, alex)@camk.edu.pl

<sup>2</sup> Universidad de Concepción, Departamento de Astronomía, Casilla 160-C,  
Concepción, Chile

<sup>3</sup> Millennium Institute of Astrophysics, Santiago, Chile

<sup>4</sup>The Observatories of the Carnegie Institution for Science, 813 Santa Barbara  
Street, Pasadena, CA 91101, USA

e-mail: ian@obs.carnegiescience.edu

<sup>5</sup> Department of Astronomy, Ohio State University, 140W. 18th Ave.,  
Columbus, OH43210, USA

e-mail: poleski.1@osu.edu

## ABSTRACT

The field of the globular cluster M10 (NGC 6254) was monitored between 1998 and 2015 in a search for variable stars. *V*-light curves were derived for 40 variables or likely variables, most of which are new detections. Proper motions obtained within the CASE project indicate that 18 newly detected variables and 14 previously known ones are members or likely members of the cluster, including one RRc-type, three type II Cepheids, and 14 SX Phe-type pulsators, one contact binary, and six semi-regular red giants. As a byproduct of the search we discovered a candidate binary comprised of main sequence stars with the record-short orbital period of 0.042 d. We also confirmed the photometric variability of the red straggler M10-VLA1 hinted at by Shishkovsky et al. (2018), who discovered this object spectroscopically. In Appendix 1 we show that CASE proper motion measurements are in a good agreement with those retrieved from the *Gaia* archive, while Appendix 2 presents evidence for low frequency  $\gamma$  Doradus-type oscillations in SX Phe stars belonging to M10.

*globular clusters: individual (M10) – stars: variables – stars: SX Phe – blue stragglers – stars: individual (M10-VLA1)*

## 1 Introduction

M10 (NGC 6254) is projected against the outskirts of the Galactic bulge at  $l = 15^\circ.1$ ,  $b = 23^\circ.1$ , in an appreciably reddened region with the total  $E(B - V)$  reddening varying between 0.26 mag and 0.29 mag across our field of view<sup>1</sup>. Its core radius  $r_c$ , half-mass radius  $r_h$ , tidal radius  $r_t$ , [Fe/H] index, radial velocity, heliocentric distance  $d_\odot$ , and galactocentric distance  $d_G$  are equal to 0'.86, 1'.81, 21'.6, -1.52,  $75.8 \pm 1.0$  km s<sup>-1</sup>, 4.3 kpc and 4.6 kpc, respectively (Harris 1996, 2010

<sup>†</sup>CASE was initiated and for long time led by our friend and tutor Janusz Kaluzny, who prematurely passed away in March 2015.

<sup>\*</sup>Based on data obtained with the Swope telescope at Las Campanas Observatory.

<sup>1</sup>The extinction calculator at <https://irsa.ipac.caltech.edu/applications/DUST/> was used for this estimate.

edition; hereafter H10).<sup>2</sup> Among globular clusters (GCs), M10 is distinguished by an almost purely blue horizontal branch (Dotter et al. 2010), and a very low specific frequency of RR Lyr-type variables:  $S_{RR} = 1.1$ , where

$$S_{RR} = N_{RR} 10^{0.4(7.5 + M_{Vt})},$$

$N_{RR}$  is the number of RR Lyrs, and  $M_{Vt}$  is the integrated  $V$ -band luminosity of the cluster (H10). The mass of M10 and its present relaxation time at  $r_h$  are estimated to be  $1.55 \times 10^5 M_\odot$ , and 743 Myr, respectively (Webb et al. 2017). The latter authors find the degree of mass segregation and the global mass function of the cluster to be consistent with its dynamical age, which makes M10 to be the only GC with a well understood dynamical history in the sample they study.

Even though M10 is as close to the Sun as 47 Tuc (H10), it has been much less extensively explored. Pre-CCD searches for variables, summarized by Clement et al. (2001, 2017 edition<sup>3</sup>; hereafter C17), resulted in the detection of just four variable objects. Within the targeted CCD surveys performed so far (von Braun et al. 2002, Salinas et al. 2016; hereafter S16) additional 15 variables were found in the cluster field, including three clear nonmembers. Blue straggler stars (BSS) in M10 were investigated by Dalessandro et al. (2011, 2013). Those authors identified 120 candidate BSS, however the time-coverage of their data was insufficient for an accompanying variability study. Pietrukowicz et al. (2008) searched the cluster for dwarf novae, but none was found. Finally, a radio-bright red straggler suspected of photometric variability has recently been discovered in M10 by Shishkovsky et al. (2018; hereafter S18).

Our survey is a part of the CASE project (Kaluzny et al. 2005) conducted using telescopes of the Las Campanas Observatory, and its aim is to increase the inventory of variable objects in the field of M10. In Section 2 we briefly report on the observations, explain the methods used to calibrate the photometry, and briefly introduce methods employed to identify variable stars. Newly discovered variables are presented and discussed in Section 3, whereas Section 4 contains new data on previously known variables which we consider worthy of publishing. For all the variables the membership probability is given based of proper motion measurements of Narloch et al. (2017; hereafter N17). The paper is summarized in Section 5, and in Appendix 1 proper motions of N17 are compared to those retrieved from the *Gaia* archive.

## 2 Observations and data processing

The present paper is mainly based on images acquired on the 1.0-m Swope telescope equipped with the  $2048 \times 3150$  pixel SITe3 camera which provided a field of view  $14.8 \times 22.8$  arcmin<sup>2</sup> at a scale of 0.435 arcsec/pixel. The data were collected during two seasons, 1998 and 2002, comprising 32 nights between May 1998 and June 2002. Additional observations were performed during seven nights starting from June 28, 2015. A new E2V camera was used, with the same scale of 0.435 arcsec/pixel, and with a field of view subrastered from the original  $29.7 \times 29.8$  arcmin<sup>2</sup> to that of SITe3. The same set of filters was always used. The seeing ranged from 1''.2 to 3''.2 and 1''.2 to 2''.5 for  $V$  and  $B$  frames, respectively, with median values of 1''.4 and 1''.5. For the analysis, 1207  $V$ -band images and 161  $B$ -band images were selected.

<sup>2</sup>Webpage <http://vizier.u-strasbg.fr/viz-bin/VizieR?~source=VII/202>.

<sup>3</sup>Webpage <http://www.astro.utoronto.ca/~cclement/cat/C1654m040>.

The photometry was performed using an image subtraction technique implemented in the DIAPL package.<sup>4</sup> To reduce the effects of PSF variability, each frame was divided into  $4 \times 6$  overlapping subframes. The reference frames were constructed by combining 11 images in  $V$  and 4 in  $B$  with an average seeing of  $1''.22$  and  $1''.23$ , respectively. The light curves derived with DIAPL were converted from differential counts to magnitudes based on profile photometry and aperture corrections determined separately for each subframe of the reference frames. To extract the profile photometry from reference images and to derive aperture corrections, the standard Daophot, Allstar and Daogrow (Stetson 1987, 1990) programs were used. Profile photometry was also extracted for each individual image, enabling useful photometric measurements of stars which were overexposed on the reference frames.

## 2.1 Photometric calibration and search for variability

The calibration of SITe3 data was based on observations of 24 Landolt standards, yielding the following transformation to the standard system:

$$\begin{aligned} V &= v + 2.9236(49) + 0.0071(70) \times (b - v) \\ B - V &= 0.2349(40) + 1.0438(55) \times (b - v), \end{aligned}$$

where lower case and capital letters denote instrumental and standard magnitudes, respectively, and numbers in parentheses are uncertainties of the last significant digits. The standard SITe3 magnitudes were then used to transform the instrumental E2V values. Since M10 has a relatively loosely populated central part, we were able to reach a photometric accuracy of 0.1 mag at  $V = 21$  mag (Fig. 1).

We obtained time-series photometry for 45,942 stars brighter than  $V \sim 22$  mag, and conducted a search for periodic variables using the AOV and AOV-TRANS algorithms implemented in the TATRY code (Schwarzenberg-Czerny 1996 and 2012; Schwarzenberg-Czerny & Beaulieu 2006).

## 3 Variable stars and their membership in M10

Membership of the cluster was assigned based on i) proper motions (PM) measured by N17, ii) angular distances from the center of the cluster, and iii) CMD locations combined with the variability type. Details concerning PM measurements and calculations of membership class  $C_{PM}$  and membership probability  $P_{PM}$  are given in N17, who also provide a PM catalog for nearly 450000 stars in the fields of 12 GCs. As detailed Appendix 1, their PMs of M10 variables generally agree with those of *Gaia*, discrepant values being obtained for two objects only. We consider a variable to be a member or likely member of the cluster if one of the following criteria is fulfilled:

1.  $P_{PM} \geq 70\%$ .
2.  $P_{PM} < 70\%$ ,  $C_{PM} = 1$  or 2, CMD-location compatible with cluster membership, variability type compatible with CMD-location, and geometric membership probability  $P_{geom} = 1 - \pi r^2 / S > 90\%$ , where  $r$  is star's angular distance from the center of M10 ( $\alpha = 16^h 57^m 09^s.05$ ,  $\delta = -04^\circ 06' 01''.1$ ) in arcseconds, and  $S = 1.22 \times 10^6$  is the size of the field of view in arcseconds<sup>2</sup>.

---

<sup>4</sup>Available from <http://users.camk.edu.pl/pych/DIAPL>

3. Proper motion not known, but  $P_{geom} > 70\%$ , CMD-location compatible with cluster membership, and variability type compatible with CMD-location.

Light curves were obtained for all the known variables within our field of view, and for 24 new variable or likely variable stars, 18 of which are PM or likely PM-members of M10. Membership status was also assigned to the variables previously discovered.<sup>5</sup>

The color-magnitude diagram (CMD) of the observed field, constructed based on the reference images, is shown in Fig. 2. To make it readable, stars with proper motions measured by N17 were only selected to serve as a background against which the variables are plotted. Stars identified by N17 as PM-members of the cluster are shown in the right panel.

Basic data for the variables are given in Table 3. For our naming convention to agree with that of C17 we start numbering the new variable cluster members from V17. The stars whose PM indicate that they do not belong to M10 are given names from N1 on. The equatorial coordinates for epoch J2000 are given in columns 2 and 3. They conform to the UCAC4 system (Zacharias et al. 2013), and are accurate to  $0''.2 - 0''.3$  (statistical  $1-\sigma$  errors). The  $V$ -band magnitudes in column 4 correspond to the maximum light in the case of eclipsing binaries, and the average magnitude is given for the remaining cases. Columns 5–7 give  $B - V$  color, amplitude in the  $V$ -band, and period of variability.

Fig. 3 shows the CMD of M10 with identifications of variable stars. PM-members of the cluster are marked in red, field stars in black, and two objects with discrepant PMs - in blue. The gray background stars are the PM-members of M10 from the right panel of Fig. 2. In the following, we describe the new variables whose light curves are shown in Figs. 5 and 6.

### 3.1 Cluster members

The blue stragglers V17 – V20 are SX Phe-type pulsators. Multimodal pulsations are observed for V17 and V19, and are likely for V18 (in all three cases the appreciable dispersion of the light-curve in Fig. 5 is at least partly caused by or can be at least partly attributed to amplitude variations). V20 in turn is a showcase example of a High Amplitude  $\delta$  Scuti-type variable with an amplitude of  $\sim 0.5$  mag and a very stable, apparently single-mode light curve. All four of these stars are 100% PM-members of M10. However, V19 is located unusually far from the center of the cluster for a blue straggler (at  $\sim 4.4r_h$ ), so that in principle it might be a field  $\delta$  Sct star. A radial velocity measurement would be needed to confirm its membership.

V21, another 100% PM-member of the cluster, is the only W UMa-type variable detected in M10. Judging from Fig. 1, we should have easily detected W UMas brighter than  $V \approx 19$  mag with an amplitude larger than  $\sim 0.1$  mag, but none were found. The apparent paucity of contact binaries in M10 compared to other clusters surveyed within CASE (e.g. 16 confirmed, 1 confirmed + 7 likely, 3 confirmed + 1 likely, 7 confirmed + 1 likely, and 10 confirmed, respectively in M22, NGC 3201, NGC 362, NGC 6362, and M4) is puzzling. Underrepresented W UMas together with numerous blue stragglers, at least some of which should have originated from merged binaries (e.g. Li et al. 2018), suggest that - contrary to the conjecture of Webb et al. (2017) - M10 may have an interesting dynamical history. Contact systems in GCs are generally not found significantly

<sup>5</sup>Data for all the identified variables are available at <http://case.camk.edu.pl>

below the main-sequence turnoff, a possible explanation being that they form primarily due to nuclear evolution of detached binaries, and a contact configuration is achieved once the more massive component exhausts hydrogen in the core and starts to expand (e.g. Kaluzny et al. 2016). V21 is only the second exception to this rule, the first one being KT-08 in M22 (Rozycka et al. 2017).

V22, the only RR Lyr-type variable found in M10, has a light curve characteristic of first overtone (i.e. RRc) pulsators. It exhibits a moderate Blazhko effect, and in the CMD of the cluster it resides close to the blue edge of the instability strip.

The low-amplitude sinusoidal light curve of V23 may originate from the reflection effect. Since the star is located in a rather loosely populated area beyond  $r_h$ , there should be no problem with a spectroscopic verification of this possibility.

V24 is a BL Her-type pulsator, and the third type II Cepheid in M10 after V2 and V3 cataloged by C17. Among these objects it has the lowest luminosity and the shortest period ( $P = 2.31$  d).

The semi-regular variable V25 is located on the blue horizontal branch (BHB), which makes its 4.46 day variability difficult to understand. Its light curve seems too irregular to be caused by the reflection effect. In the Swope frames there is no trace of blending, but in principle it may be tightly blended with a field binary. Unfortunately, no HST imaging data of M10 are available at its location at  $\sim 1.3r_h$ , and the only means to verify the nature of this object is spectroscopy.

V26 is a red straggler with a sinusoidal light curve and possible secular changes of the average brightness. As such, it photometrically resembles V34 described below. The phase of the sinusoid is preserved throughout 1998 and 2002 seasons, and most likely until the 2015 season, which suggests a stable orbital origin of the variations, and makes V26 interesting for spectroscopic observations.

PM-members V27, V28, V29 and the likely member V30 are long period semi-regular red giants with amplitudes of a few tenths of a magnitude. V27, V28 and V30 reside within  $r_h$ ; V29 is located in the outer part of M10 at  $\sim 3.5R_h$ . In the CMD the four objects are clustered at the red giant tip next to V1 which was discovered in mid-50's, and one may wonder how they escaped detection for over 60 years.

Suspected variables V31, V32 and V33 exhibit low-amplitude, roughly sinusoidal variations of unknown origin which should be independently confirmed.

V34 is a likely member of M10 and an optical counterpart of the radio- and X-ray active object M10-VLA1 studied by S18. Throughout all three seasons it exhibits variations which can be phased with the spectroscopic period of 3.3391 d found by S18 (see Fig. 7; we note that  $P = 3.3389$  d seems to fit the light curve slightly better while preserving the overall agreement with the radial velocity data). The shape and amplitude of the light curve vary from season to season, thus confirming the conclusion of S18 who classify this object as an interacting binary. According to S18, the observed properties of M10-VLA1 are consistent with a black hole primary, with the exception of the low mass function which requires a statistically unlikely, nearly face-on orientation. Assuming that the photometric variability originates predominantly from the reflection effect, we tried to model the light curve with the PHOEBE implementation of the Wilson–Devinney code (Prša and Zwitter 2005), the effect itself being simulated by a hot spot on the surface of the secondary. We found it possible to reasonably fit the light curve even for an orbital inclination of 4 deg. However,

the hot spot has to be placed at an orbital longitude of  $\sim 90^\circ$ , which is a physically unlikely location. Thus, either the photometric variations originate predominantly somewhere else in the system (e.g. in an accretion disk around the primary), or the alternative possibility suggested by S18 is true, namely that M10-VLA1 is an extreme flaring RS CVn system (note that, since we do not observe eclipses, its orbital period could be different from the spectroscopic period of S18). In any case, this object certainly deserves a detailed multi-wavelength study.

### 3.2 Field variables

N1 is a background SX Phe or  $\delta$  Sct-type high-amplitude pulsator discovered by von Braun et al. (2002) who refer to it as V3 in their paper. We confirm the period they found, and find the pulsations to be likely multimodal.

Based solely on its CMD-location, the contact binary N2 could in principle belong to M10. Its proper motion is unknown, but its large distance from the center of the cluster (almost  $6r_h$ ) indicates that it is a background object.

N3 is an RRc-type pulsator with possible Blazhko effect variations. The CMD-location and proper motion indicate it is another background object.

The proper motions of N4 and N5 identify them as field objects. N5 is most probably a background red giant similar to V3 (see Fig. 8), while the nature of the low-amplitude sinusoidal variability of N4 is unclear. The variability might arise from the reflection effect, but additional data are needed to verify such a possibility.

N6, a marginally detected eclipsing binary with an amplitude of  $\sim 0.3$  mag and a period of only 0.042 d (60.5 minutes), is so weak in the  $B$ -band that we could not detect it in our frames. N17 were not able to derive its proper motion, but a simple reasoning shows that it cannot belong to M10. If it were a member of the cluster then with  $A_V = 3 \times 0.28 = 0.84$  mag its absolute magnitude in the  $V$ -band would amount to 8.1 mag. The light curve is compatible with that generated by a pair of nearly identical stars. Assuming they are indeed identical, each of the components would have  $M_V = 8.85$  mag, corresponding to  $\mathcal{M} = 0.60 M_\odot$  and  $R = 0.56 R_\odot$  (Pecaut, Mamajek & Bubar 2012, 2018 edition<sup>6</sup>; hereafter PMB18). For this mass and  $P = 0.042$  d we get an orbital separation  $a = 0.54 R_\odot$  - much too small to accommodate two  $R = 0.56 R_\odot$  components. Since for low-mass stars  $R$  scales roughly proportionally to  $\mathcal{M}$ , while at a fixed  $P$   $a \propto \mathcal{M}^{1/3}$ , the components of N6 must be much less massive than  $0.60 M_\odot$ , which implies that the binary must be located much closer to the Sun than M10. For  $\mathcal{M} = 0.12 M_\odot$  we obtain  $a = 0.32$  and  $R = 0.15 R_\odot$  (PMB18), i.e. a nearly contact configuration which would have the observed  $m_V = 22.1$  mag if it was located at 340 pc from the Sun. Neglecting absorption, this is the maximum distance allowed by our data. Still less massive configurations would have to be located correspondingly closer to the Sun, down to  $\sim 45$  pc for  $\mathcal{M} = 0.08 M_\odot$ . The shortest orbital period reported so far for a binary composed of main-sequence stars is 0.098 d for OGLE-BLG-ECL-000066 (Soszyński et al. 2015). Since N6 would become the next record holder if its variability was confirmed, it clearly deserves a dedicated observational effort.

---

<sup>6</sup>Webpage: [http://www.pas.rochester.edu/~emamajek/EEM\\_dwarf\\_UBVIJHK\\_colors\\_Teff.txt](http://www.pas.rochester.edu/~emamajek/EEM_dwarf_UBVIJHK_colors_Teff.txt)

## 4 New data on known variables

The red giants V1, V2 and V3 have rather stable, roughly sinusoidal light curves (Fig. 8), suggesting that their variability originates primarily from pulsations or long-living spots.

V4, cataloged by C17 as a possible RR Lyr-type variable, is in fact constant with an accuracy of 0.01 mag in *V*-band. As a PM-member of M10 it is interesting because of its CMD-location in the instability strip, slightly redward from the genuine RR Lyr-type variable V22. Since *Gaia*'s photometry confirms our findings, the pair becomes an interesting target for a follow-up study aimed at explaining why V22 does pulsate, while V4 does not.

V5 – V15 were identified by S16 as SX Phe-type pulsators which, with a possible exception of V9, belonged to M10. According to our criteria, the only nonmember of the cluster is V11, which we tentatively classify as a foreground  $\delta$  Sct-type variable. We confirm the very short period and complex nature of the V10 pulsations found by S16, however in the  $V/(B-V)$  plane this star is located among the BSS rather than midway between the turnoff and the BHB tip as in their  $i/(g-i)$  diagram. A similar mismatch occurs for V9 which according to S16 belongs to the BHB, whereas we find it in the area occupied by the BSS. An inspection of archival HST frames reveals V9 and V10 as tight ( $<0''.5$ ) blends of nearly equally bright stars. Such blended pairs are likely to have highly nonstandard colors, which could account for the observed discrepancies. For all the remaining objects from the V5 – V15 group the CMD-locations of S16 agree reasonably well with ours.

For V16 a steady increase in brightness of  $\sim 0.02$  mag was observed by S16 throughout the 6.65 hour time span of their observations on HJD 2457224. Our data show periodic variations with  $P = 0.36$  d and an amplitude of a few hundredths of a magnitude, but in the 2015 season only (HJD 2457190 – 2457201). Because of incomplete phase coverage we cannot be 100% sure about their reality. We note that in archival HST frames V16 splits into three objects, and the suspected variability may originate in one of the weaker stars of the trio.

## 5 Summary

Our photometric survey of the field of the globular cluster M10 resulted in the discovery of 24 new variable or likely variable stars, 18 of which are PM-members of the cluster. Cluster membership was confirmed for 14 out of 16 variables cataloged earlier by C17. M10 harbors a rich population of blue stragglers, however we did not find any eclipsing binaries among them, unique among clusters studied so far within CASE, i.e. NGC 6752 (Kaluzny & Thompson 2009), M55 (Kaluzny et al. 2010), M4 (Kaluzny et al. 2013), NGC 6362 (Kaluzny et al. 2014), M12 (Kaluzny et al. 2015), NGC 3201 (Kaluzny et al. 2016), NGC 362 (Rozyczka et al. 2016) and M22 (Rozyczka et al. 2017). A total of 13 blue stragglers (nine known and four newly discovered) are identified as SX Phe-type pulsators, most of these are multimodal (see Appendix 2 for a detailed discussion). We stress that in the whole cluster just one eclipsing binary was found, suggesting a peculiar dynamical history for M10.

Stars V4 and V22 share a nearly common location in the CMD close to the edge of the instability strip, however only V22 is found to pulsate. A more accurate photometric follow-up is desirable to precisely determine their magnitudes and colors. If their location close to each other in the CMD is confirmed, a

detailed study should be undertaken to explain why V4 does not vary.

We provide a light curve of V34 – the optical counterpart of the radio and X-ray source M10-VLA1 discovered spectroscopically by S18 – obtained over three observing seasons, and we argue that the observed variability is unlikely to originate from the reflection effect. Another interesting object, N6, is a marginally detected eclipsing system with  $P = 0.042$ d which, if confirmed, will have the record-short orbital period among binaries with main-sequence components.

Finally, the three type II Cepheids V2, V3 and V24 represent three distinct evolutionary stages corresponding to three different crossings of the instability strip.

**Acknowledgments.** We thank Grzegorz Pojmański for the lc code which vastly facilitated the work with light curves. ASC acknowledges partial funding from NCN grant 2016/23/B/ST9/03123. This work is partly based on data from the European Space Agency (ESA) mission *Gaia* (<https://www.cosmos.esa.int/gaia>), processed by the *Gaia* Data Processing and Analysis Consortium (DPAC, <https://www.cosmos.esa.int/web/>). Funding for the DPAC has been provided by national institutions, in particular the institutions participating in the *Gaia* Multilateral Agreement. We also made use of the Mikulski Archive for Space Telescopes (MAST). STScI is operated by AURA, Inc., under NASA contract NAS5-26555. Support for MAST for non-HST data is provided by the NASA Office of Space Science via grant NNX09AF08G and by other grants and contracts.

## REFERENCES

- Barceló F. S., Roca C. T., García H. A., and García, R. A. 2017, *Astron. Astrophys.*, **601**, A57.
- Clement, C. M., Muzzin, A., Dufton, Q., Ponnampalam, T., Wang, J. et al. 2001, *Astron. J.*, **122**, 2587 (C17).
- Dalessandro, E., Lanzoni, B., Beccari, G., Sollima, A., Ferraro, F. R., and Pasquato, M. 2011, *Astrophys. J.*, **743**, 11.
- Dalessandro, E., Ferraro, F. R., Lanzoni, B., Schiavon, R. P., O’Connell, R.W. and Beccari, G. 2013, *Astrophys. J.*, **770**, 11.
- Dotter, A., Sarajedini, A., Anderson, J., Aparicio, A., Bedin, L. R. et al. 2010, *ApJ*, **708**, 698.
- Grigahcene, A., Antoci, V., Balona, L., Catanzaro, G., Daszynska-Daszkiewicz, J. et al. 2010, *Astrophys. J.*, **713**, 192.
- Guo, Z., Gies, D. R., and Matson, R. A. 2017, *Astrophys. J.*, **851**, 39.
- Harris, W.E. 1996, *Astron. J.*, **112**, 1487 (H10).
- Kaluzny, J. 2000, *ASP Conf. Ser.*, **203**, 19.
- Kaluzny, J., Rozycka, M., Thompson, I. B., Narloch, W., Mazur, B. et al. 2016, *Acta Astron.*, **66**, 31.
- Kaluzny, J., and Thompson, I. B. 2009, *Acta Astron.*, **59**, 273.
- Kaluzny, J., Thompson, I. B., Krzeminski, W., Preston, G. W., Pych, W. et al. 2005, *Stellar Astrophysics with the World’s Largest Telescopes, AIP Conf. Proc.*, **752**, 70.
- Kaluzny, J., Thompson, I. B., Krzeminski, W., and Zloczewski, K. 2010, *Acta Astron.*, **60**, 245.
- Kaluzny, J., Thompson, I.B., Narloch, W., Pych, W., and Rozycka, M. 2015, *Acta Astron.*, **65**, 267.
- Kaluzny, J., Thompson, I. B., Rozycka, M., and Krzeminski, W. 2013, *Acta Astron.*, **63**, 181.
- Kaluzny, J., Thompson, I. B., Rozycka, M., Pych, W., and Narloch, W. 2014, *Acta Astron.*, **64**, 309.
- Kurtz, Donald W., Shibahashi, H., Murphy, S. J., Bedding, T. R., Bowman, D. M. 2015, *MNRAS*, **450**, 3015.
- Li, C., Deng, L., de Grijs, R., Jiang, D., and Xin, Y. 2018, *Astrophys. J.*, **856**, 25.
- Mazur, B., Krzeminski, W., and Thompson, I.B. 2003, *MNRAS*, **340**, 1205.
- Narloch, W., Kaluzny, J., Poleski, R., Rozycka, M., Pych, W., and Thompson, I. B. 2017, *MNRAS*, **471**, 1446. (N17)
- Nemec, J. M., Balona, L. A., Murphy, S. J., Kinemuchi, K., Jeon, Y.-B. 2017, *MNRAS*, **466**, 1290. (NB17)



- Pancino E., Bellazzini M., Giuffrida G., and Marinoni S. 2017, *MNRAS*, **467**, 412.
- Pecaut, M. J., Mamajek, E. E., and Bubar, E. J. 2012, *Astrophys. J.*, **746**, 154 (PMB18).
- Pietrukowicz, P., Kaluzny, J., Schwarzenberg-Czerny, A., Thompson, I. B., Pych, W. et al. 2008, *MNRAS*, **388**, 1111.
- Prša, A., and Zwitter, T. 2005, *Astrophys. J.*, **628**, 426.
- Rozyczka, M., Thompson, I.B., Narloch, W., Pych, W., and Schwarzenberg-Czerny, A. 2016, *Acta Astron.*, **66**, 307.
- Rozyczka, M., Thompson, I.B., Pych, W., Narloch, W., Poleski, R., and Schwarzenberg-Czerny, A. 2017, *Acta Astron.*, **67**, 203.
- Salinas, R., Contreras Ramos, R., Strader, J, Hakala, P., Catelan, M. et al. 2016, *Astron. J.*, **152**, 55 (S16).
- Schwarzenberg-Czerny, A. 1991, *MNRAS*, **253**, 198.
- Schwarzenberg-Czerny, A. 1996, *Astrophys. J. Letters*, **460**, L107.
- Schwarzenberg-Czerny, A. 2012, *New Horizons in Time-Domain Astronomy, IAU Symposium*, **285**, 81.
- Schwarzenberg-Czerny A., and Beaulieu, J.-Ph. 2006, *MNRAS*, **365**, 165.
- Shishkovsky, L., Strader, J., Chomiuk, L., Bahramian, A., Tremou, E. et al. 2018, *Astrophys. J.*, **855**, 55 (S18).
- Soszyński, I., Stępień, K., Pilecki, B., Mrz, P., Udalski, A. et al 2015, *Acta Astron.*, **65**, 39.
- Stetson, P. B. 1987, *P.A.S.P.*, **99**, 191.
- Stetson, P. B. 1990, *P.A.S.P.*, **102**, 932.
- von Braun, K., Mateo, M, Ciboucas, K., and Athey A. 2002, *Astron. J.*, **124**, 2067.
- Webb, J. J., Vesperini, E., Dalessandro, E., Beccari, G., Ferraro, F., and Lanzoni, B 2017, *MNRAS*, **471**, 3845.
- Zacharias, N., Finch, C. T., Girard, T. M., Henden, A., Bartlett, J. L. et al. 2013, *Astron. J.*, **145**, 44.

## Appendix 1: CASE and *Gaia* PM-measurements

N17 measured proper motions for 33 of the variables presented here, for 29 of which *Gaia* measurements are also available. To enable a comparison of the two sets of results, the absolute *Gaia* PMs were transformed to the cluster frame iteratively. First, three evident nonmembers (N3, N4 and N5) were rejected, an approximate location of the cluster center on the  $(\mu_\alpha, \mu_\delta)$  plane was found, and PMs relative to it were calculated. Stars with total PMs larger than  $2 \text{ mas y}^{-1}$  (V8 and V9) were then rejected, and the last two steps were repeated. The resulting absolute PM of M10 was equal to  $(-4.76, -6.67) \text{ mas y}^{-1}$ , well agreeing with  $(-4.82, -6.18) \text{ mas y}^{-1}$  obtained by N17.

A graphical comparison of proper motions derived by N17 with those of *Gaia* is presented in Fig. 9. For N4 and N5, which move most rapidly with respect to M10, the quantitative agreement is excellent, and for the slightly slower N3 it is still satisfactory. For further 24 objects a good qualitative agreement is observed in the sense that all of them occupy the same small area on the  $(\mu_\alpha, \mu_\delta)$  plane, marked in Fig. 9 with a circle. In the last two cases (V8 and V9) N17 and *Gaia* PMs are discrepant. This may be due to the fact that (as we mentioned in Section 4) V9 is a tight blend of nearly equally bright stars, whereas V8 is located at  $\sim 1.2 \text{ arcsec}$  from a star several times brighter. The median distance between CASE and *Gaia* points, taken for all objects shown in Fig. 9, amounts to  $0.75 \text{ mas}$ . The corresponding mean distance is  $1.10 \text{ mas}$  ( $0.78 \text{ mas}$  calculated without discrepant PMs).

RMS of  $\mu_\alpha$  calculated from N17 and *Gaia* data for objects within the circle in Fig. 9 amounts to  $0.60$  and  $0.54 \text{ mas y}^{-1}$ , respectively, whereas RMS of  $\mu_\delta$  - to  $0.44$  and  $0.47 \text{ mas y}^{-1}$ , respectively. At a distance of  $4.3 \text{ kpc}$  from the Sun  $1 \text{ mas y}^{-1}$  translates into  $\sim 20 \text{ km s}^{-1}$ , corresponding to an RMS of  $\sim 10 \text{ km s}^{-1}$  in  $\mu_\alpha$  or  $\mu_\delta$ . As the central radial velocity dispersion of M10 is about  $5 \text{ km s}^{-1}$  (N17 and references therein), it is clear that while N17 results

and presently available *Gaia* data suffice for the membership assignment, they are not accurate enough for a study of the internal dynamics of the cluster. An accuracy necessary to that end is only expected to be reached in the final *Gaia* releases (Pancino et al. 2017).

## Appendix 2: Variability of SX Phenicis stars in M10

SX Phoenixis pulsating stars differ from their cousins, the  $\delta$  Scuti variables by having shorter periods, lower metallicity and smaller amplitudes. They belong to population II, most are members of globular clusters, galactic halo and thick disk. There were suspicions that many very low amplitude oscillations in them remain undetected (Kaluzny, 2000, Mazur et al. 2003). Space observations confirmed that belief (Nemec et al. 2017, hereafter NB17). Since some  $\delta$  Scuti variables reveal low frequency oscillations of  $\gamma$  Doradus type, becoming hybrid pulsators, a similar behavior may be expected for SX Phenicis stars. Again, recent space observations confirmed this expectations (Guo et al. 2017, NB17).  $\gamma$  Doradus stars are high-order gravity (g) mode pulsators, permitting probing of their interiors by means of astroseismic analysis. Since in globular clusters the SX Phe stars belong to the population of blue stragglers, the detection of g-modes would provide new means to study those exotic objects. This prompted us to look more closely at 13 SX Phe stars discovered so far in M10.

### 6.1 Methods of Analysis

In analysing our sample of SX Phe pulsators one must keep in mind the peculiar form of our window function. In some years our observing runs spanned several months, so that a typical half width of 1 cycle/day (c/d) aliases is 0.01 c/d (HWHI). Nightly coverage was fairly good, so that for strong, isolated peaks there was no 1 c/d ambiguity. However, due to window function interference this does not hold for low amplitude peaks in dense spectral regions. The observations typically spanned around 1500 d (6300 d for V5) with no coverage on some years, so that no unique cycle count was possible. As a result, daily aliases split into  $\sim 5$  (or more for V5) yearly aliases of comparable height. Because of that we refrain from a discussion of mode combination and rotational splitting. Frequency and amplitude of the strongest peak are provided as they appear, ignoring yearly aliases of comparable height.

For the analysis the NFIT software package written by ASC was used. First, we calculated Analysis of Variance (AOV) frequency spectrum, and identified its strongest peaks, next we fitted the corresponding Fourier series and subtracted it from observational data to pre-whiten these frequencies. In the process we adjusted both the amplitudes and the frequencies of sine/cosine modes by a non-linear least squares procedure (NLSQ). Then the whole procedure was repeated till no significant features remained in the spectrum. At each step the results were inspected to identify the largest harmonics and/or strongly correlated modes. Finally, we performed the NLSQ fit of the original data with the grand-total model of all detected modes. The results are listed in Table 6.2. The median standard deviation of the residuals from model fits is 11 mmag.

## 6.2 Results

We list only modes with amplitudes five times larger than their LSQ errors ( $5\sigma$  criterion). For such a purpose the AOV frequency spectrum was particularly useful as it yields model to noise power ratio (Schwarzenberg-Czerny 1996). A common magnitude cut-off proved impractical, as due to the strong modulation of amplitudes and/or frequencies of some modes their errors varied considerably. Table 6.2 lists formal errors of frequencies and amplitudes returned from NLSQ procedure. Frequency errors assume a fixed cycle count and ignore year aliasing, and amplitude errors may suffer from underestimation due to correlation of residuals (Schwarzenberg-Czerny 1991). Thus, the corresponding entries in Table 6.2 should not be taken at their face values, but rather as indicators of relative fit quality of different modes.

Two frequency regions, namely the low frequency one, below 5 c/d, and the high frequency one above this limit deserve a separate discussion. On the one hand, because of our sampling pattern nothing reliable may be said on frequencies near 0 and 1 c/d ( $\pm 0.02$  c/d). In a few oscillations with frequencies lower than 1.5 c/d the poor phase coverage manifested itself by large ( $> 0.9$ ) correlation with the Fourier constant term, yet this was not common. On the other hand, at least in a half of our sample pre-whitening of several discrete low frequency modes left no power excess near zero frequency. Hence, we infer that instrumental effects did not significantly distort the power spectrum there. This is strengthened by the fact that no low frequency oscillations were detected in V12. The low-frequency part of the spectrum may be affected by variable blending effects; yet, given the fraction of variable stars of  $\sim 0.01$  in the observed field, this may not apply generally.

At higher frequencies two alternate situations emerge. In most frequency spectra one or several well separated peaks and their harmonics appear in the range above 10 c/d. On rare occasions in the region 10-30 c/d we observe one or two broad bumps several c/d wide, while little power is seen at other frequencies. Since FWHI of our daily frequency patterns is of order of 0.02 c/d, several dozens of densely packed discrete modes would be needed to produce such a feature. An alternative explanation is light curve modulation on time scales of several days, yielding a broad continuous frequency spectrum.

The amplitudes of detected pulsation modes span range from as large as 233 mmag for V20 till 2.5 mmag in V12 where scatter of observations was particularly small (Table 6.2). V8 and V19 exhibit SX Phe mode pulsation in one mode only, with a harmonic. Low frequency modulation in them is weak. In most stars the detected modes span 10-25 c/d frequency range oscillations with some harmonics detectable beyond our detection limit of 75 c/d. There is also evidence of low frequency modulation of amplitudes reaching 10 mmag and more.

The strongest evidence of modulation of oscillations is present in V5, as indicated by amplitude errors over 10 times larger than those resulting from oscillations of comparable strength in other stars. We refrain from listing frequencies of several nominal large amplitude oscillations, of order  $\sim 120$  mmag, at frequencies 0.267763, 1.269207, 10.332841, 17.361620, 40.365515 and 68.385442 c/d, because of their errors exceeding 30 mmag or more. They are either unstable, or phase and/or amplitude modulated.

Low frequency oscillations may be due to  $\gamma$  Doradus oscillations, or a combination of high frequency modes with rotation/orbital modulation. Both the base frequency 1.09 c/d and its harmonic are detected in V15. This may indi-

cate rotation modulation, and although opinions in literature differ, such a value is consistent with already observed elsewhere (NB 2017, Kurtz et al, 2015). In three stars, namely V10, V13 and V18, the low amplitude modulation amplitude dominate those of high frequency modes. This seems to exclude an origin due to combination of high frequency modes. The presence of two such modes in V13 excludes the rotation interpretation, independently on whether the true frequency of the stronger mode is closer to 1 or 0 c/d. The remaining explanation is: we see  $\gamma$  Dor oscillations. Similarly, in Kepler power spectra of 9244992, 6780873, and 5390069 in NB17 two strong low frequency peaks appear without evidence of candidate combination peaks at high frequencies. Because of number, variety and strength of features observed in M10 at frequencies below 5 c/d it is hard to avoid the conclusion that while most of them occur due to combination of higher frequency modes (in accordance with Kurtz et al. 2015), some of them are gravity modes of  $\gamma$  Dor type.

In several stars, notably V5, V10, V17, V18 and V19 broad low amplitude bumps still remain in the pre-whitened frequency spectrum after removal of all identified discrete frequencies. They spread over the typical range of SX Phe base frequencies, sometimes reaching the harmonic region of 50 c/d. Hence, they seem to be a genuine effect of stellar origin, similar to observed in some  $\delta$  Scuti stars (Barceló et al. 2017). If so, they may correspond to chaotic instability/modulation over a time interval of several base mode cycles. Summarising, our observations reveal low frequency oscillations due to either  $\gamma$  Dor or combination modes, strong modulation of SX Phe oscillations and instability of those modes on time scales as short as days in the extreme.

Table 3: Basic data of the variables identified in the M10 field

ID	RA <sub>J2000</sub> [deg]	DEC <sub>J2000</sub> [deg]	V [mag]	B - V [mag]	$\Delta_V$ [mag]	Period [d]	Type <sup>a</sup>	M <sup>b</sup>
V1	254.29214	-4.09336	11.83	1.52	0.56	70.878903	SR	Y
V2	254.29891	-4.06658	12.05	0.96	1.18	19.470995	W Vir	Y
V3	254.23315	-4.07123	12.75	0.87	0.47	7.872181	W Vir	Y
V4	254.31004	-4.18284	14.74	0.53	—	—	<i>const</i>	Y
V5	254.28580	-4.10453	16.97	0.44	0.55	0.058543	SX	Y
V6	254.29457	-4.09261	16.69	0.51	0.20	0.059909	SX	Y
V7	254.29321	-4.11758	17.48	0.50	0.09	0.048112	SX	Y
V8	254.28491	-4.08576	16.99	0.46	0.11	0.051009	SX	Y*
V9	254.29404	-4.09771	17.20	0.68	0.27	0.051301	SX?	Y*
V10	254.28512	-4.11522	17.39	0.63	0.08	0.022319	SX	Y
V11	254.29507	-4.09886	16.91	0.80	0.13	0.047957	DS	N
V12	254.27108	-4.10487	17.18	0.43	0.04	0.022823	SX	Y
V13	254.28890	-4.06591	16.89	0.48	0.06	0.036174	SX	Y
V14	254.28831	-4.10149	17.32	0.46	0.09	0.038198	SX	Y
V15	254.30533	-4.09694	17.44	0.53	0.07	0.034835	SX	Y
V16	254.27802	-4.14490	16.76	0.92	0.03	0.357809	<i>susp</i> <sup>c</sup>	Y
V17	254.27298	-4.12981	17.24	0.52	0.09	0.036944	SX	Y
V18	254.33431	-4.08116	17.51	0.50	0.05	0.042435	SX	Y
V19	254.41109	-4.14928	17.61	0.53	0.06	0.043795	SX	Y
V20	254.26237	-4.06683	16.97	0.44	0.51	0.050603	SX	Y
V21	254.31559	-4.10557	19.31	0.86	0.21	0.244976	EW	Y
V22	254.28467	-4.03882	14.62	0.47	0.34	0.404604	RRc	Y
V23	254.26299	-4.13106	17.58	0.53	0.06	1.446583	<i>sin</i>	Y
V24	254.28146	-4.09510	13.95	0.76	0.35	2.307458	BL Her	Y
V25	254.27427	-4.06279	17.41	-0.02	0.07	4.457001	SR	Y
V26	254.30499	-4.06993	16.36	1.04	0.29	21.784707	<i>sin</i>	Y
V27	254.31281	-4.09790	11.91	1.89	0.28	21.004000	SR	Y
V28	254.29483	-4.07884	11.90	1.83	0.25	60.483833	SR	Y
V29	254.36407	-4.02354	11.87	1.76	0.58	68.388291	SR	Y
V30	254.28242	-4.10166	12.43	1.42	0.24	71.667981	SR	Y
V31	254.25264	-4.07014	15.92	0.09	0.07	0.205066	<i>sin, susp</i>	Y
V32	254.36188	-4.07538	17.93	0.73	0.04	0.848041	<i>sin, susp</i>	Y
V33	254.34408	-4.05701	17.56	0.00	0.09	0.933530	<i>sin, susp</i>	Y
V34	254.29489	-4.14371	17.01	0.91	0.16	3.339100	<i>sin</i> <sup>d</sup>	Y
N1	254.20253	-3.97676	19.64	0.43	0.34	0.063696	DS <sup>e</sup>	N
N2	254.27678	-3.92101	20.10	1.11	0.35	0.268554	EW	N
N3	254.34280	-4.08330	16.54	0.48	0.42	0.294384	RRc	N
N4	254.27512	-4.23526	16.74	1.64	0.08	2.111434	<i>sin</i>	N
N5	254.27756	-4.21678	18.00	1.16	0.24	6.766509	<i>sin</i>	N
N6	254.27708	-4.01820	22.10	—	0.30	0.041981	EA/EB	N

<sup>a</sup> EA - detached eclipsing binary, EB - type  $\beta$  Lyr eclipsing binary, EW - contact binary; SX, DS, RRc, W Vir and BL Her - pulsators of SX Phe,  $\delta$  Sct, RR Lyr c, W Vir and BL Her type, *sin* - sinusoidal light curve of unknown origin, *susp* - suspected variable, *const* - no variability detected.

<sup>b</sup> Membership status according to N17: Y - member or likely member (starred: discrepant CASE and *Gaia* proper motions; see Appendix), N - field object.

<sup>c</sup> Variability detected in 2015 only. <sup>d</sup> M10-VLA1 (S18). <sup>e</sup> V3 of von Braun et al. (2002).

Table 1: Pulsation frequencies detected in SX Phe stars

Id	Frequency [c/d]	Ampl. [mmag]	Id	Frequency [c/d]	Ampl. [mmag]
V5			V8		
f <sub>1</sub>	0.623036 (6)	49.5(3.7)	f <sub>1</sub>	1.744487 (71)	4.5(0.7)
f <sub>2</sub>	1.011843 (9)	34.6(4.3)	f <sub>2</sub>	19.604362 (7)	44.7(0.6)
f <sub>3</sub>	1.424943 (12)	22.9(3.7)	2f <sub>2</sub>	39.208725 -	9.9(0.6)
f <sub>4</sub>	1.980009 (10)	22.3(3.8)	3f <sub>2</sub>	58.813087 -	4.8(0.6)
f <sub>5</sub>	2.205710 (6)	32.0(3.4)	V10		
2f <sub>5</sub>	4.411421 -	16.2(3.1)	f <sub>1</sub>	0.642146 (28)	11.3(1.1)
f <sub>6</sub>	5.809590 (9)	24.9(3.0)	f <sub>2</sub>	1.005681 (33)	19.1(2.3)
f <sub>7</sub>	12.180899 (11)	18.3(3.0)	2f <sub>1</sub>	1.284291 -	5.5(1.0)
f <sub>8</sub>	17.077723 (5)	54.1(4.5)	f <sub>3</sub>	14.617339 (111)	4.0(0.8)
f <sub>9</sub>	17.079976 (1)	211.2(4.8)	f <sub>4</sub>	19.442675 (152)	4.0(0.8)
f <sub>10</sub>	21.884772 (6)	38.2(3.1)	f <sub>5</sub>	39.761490 (28)	14.6(0.8)
f <sub>11</sub>	23.820710 (11)	17.2(3.2)	f <sub>6</sub>	42.742695 (87)	5.1(0.8)
2f <sub>9</sub>	34.159952 -	47.5(3.0)	f <sub>7</sub>	44.805034 (25)	18.2(0.8)
f <sub>12</sub>	34.549065 (11)	17.6(3.0)	f <sub>8</sub>	49.849907 (103)	3.5(0.7)
f <sub>13</sub>	35.162365 (13)	12.9(2.7)	V12		
f <sub>14</sub>	38.964097 (6)	31.4(2.9)	f <sub>1</sub>	22.717670 (41)	2.9(0.4)
3f <sub>9</sub>	51.239928 -	20.8(3.0)	f <sub>2</sub>	29.509114 (49)	2.5(0.4)
f <sub>15</sub>	56.044101 (10)	18.8(3.0)	f <sub>3</sub>	43.782017 (24)	4.9(0.4)
V6			V13		
f <sub>1</sub>	0.474062 (30)	7.4(1.2)	f <sub>1</sub>	1.004305 (37)	10.5(1.5)
f <sub>2</sub>	0.975011 (8)	28.2(1.3)	f <sub>2</sub>	1.129659 (66)	5.2(0.8)
f <sub>3</sub>	1.610948 (13)	16.3(0.9)	f <sub>3</sub>	1.360120 (41)	9.6(0.9)
f <sub>4</sub>	2.276423 (24)	10.0(0.9)	f <sub>4</sub>	9.087800 (86)	3.3(0.7)
f <sub>5</sub>	2.372293 (21)	11.8(1.0)	f <sub>5</sub>	9.929391 (91)	3.9(0.8)
f <sub>6</sub>	2.698967 (15)	13.8(0.9)	f <sub>6</sub>	21.471789 (73)	5.3(0.8)
f <sub>7</sub>	9.125513 (44)	4.4(0.7)	f <sub>7</sub>	22.796205 (65)	5.8(1.2)
f <sub>8</sub>	12.368305 (46)	4.1(0.7)	f <sub>8</sub>	35.483238 (87)	4.0(0.8)
f <sub>9</sub>	13.059566 (4)	45.7(0.7)	V14		
f <sub>10</sub>	16.696109 (3)	60.5(0.8)	f <sub>1</sub>	0.643164 (34)	10.4(1.3)
f <sub>11</sub>	18.087565 (28)	7.2(0.8)	f <sub>2</sub>	0.941986 (54)	7.1(1.3)
f <sub>12</sub>	20.908996 (36)	5.4(0.7)	f <sub>3</sub>	7.469010 (60)	6.1(1.1)
f <sub>13</sub>	23.130960 (54)	3.9(0.7)	f <sub>4</sub>	23.138565 (51)	7.9(1.1)
f <sub>14</sub>	26.117025 (53)	3.8(0.7)	f <sub>5</sub>	26.145759 (29)	14.1(1.4)
f <sub>15</sub>	29.755747 (33)	5.8(0.7)	f <sub>6</sub>	26.969884 (54)	6.9(1.2)
2f <sub>10</sub>	33.392218 -	5.9(0.7)	f <sub>7</sub>	27.048688 (28)	13.7(1.4)
V7			V15		
f <sub>1</sub>	0.485023 (23)	6.4(1.4)	f <sub>1</sub>	0.975006 (37)	4.5(0.7)
f <sub>2</sub>	1.681329 (40)	4.3(0.7)	f <sub>2</sub>	1.089195 (21)	3.1(0.6)
f <sub>3</sub>	2.293711 (43)	3.6(0.6)	2f <sub>2</sub>	2.178390 -	3.7(0.6)
f <sub>4</sub>	4.961245 (53)	3.1(0.6)	f <sub>3</sub>	22.816304 (27)	5.5(0.6)
f <sub>5</sub>	20.787488 (5)	34.9(0.7)	f <sub>4</sub>	23.589314 (49)	2.9(0.6)
f <sub>6</sub>	21.348648 (50)	4.9(0.8)	f <sub>5</sub>	25.023657 (37)	3.9(0.6)
f <sub>7</sub>	21.389382 (25)	9.8(0.7)	f <sub>6</sub>	27.784002 (48)	3.3(0.6)
f <sub>8</sub>	40.818834 (48)	3.6(0.7)	f <sub>7</sub>	28.706828 (8)	19.5(0.6)
f <sub>9</sub>	46.769927 (50)	3.2(0.6)	f <sub>8</sub>	29.581976 (19)	8.0(0.6)

Table 2: Pulsation frequencies detected in SX Phe stars

Id	Frequency [c/d]		Ampl. [mmag]	Id	Frequency [c/d]		Ampl. [mmag]
V17				V20			
f <sub>1</sub>	0.028952	(20)	8.6(0.7)	f <sub>1</sub>	0.004405	(27)	7.5(0.7)
f <sub>2</sub>	0.393907	(24)	5.7(0.6)	f <sub>2</sub>	0.121073	(25)	5.5(0.6)
f <sub>3</sub>	2.038169	(49)	3.1(0.6)	f <sub>3</sub>	2.269694	(45)	3.1(0.5)
f <sub>4</sub>	27.066525	(4)	30.8(0.5)	f <sub>4</sub>	6.629676	(43)	3.2(0.5)
f <sub>5</sub>	27.611165	(42)	3.3(0.6)	f <sub>5</sub>	19.112973	(12)	5.1(0.6)
f <sub>6</sub>	27.786646	(13)	8.3(0.5)	f <sub>6</sub>	19.761623	(1)	233.2(0.5)
f <sub>7</sub>	52.283249	(25)	5.5(0.5)	f <sub>7</sub>	20.441022	(39)	3.5(0.5)
2f <sub>4</sub>	54.133050	-	2.9(0.5)	f <sub>8</sub>	26.356067	(19)	7.3(0.5)
2f <sub>6</sub>	55.573291	-	2.8(0.5)	f <sub>9</sub>	37.135945	(39)	3.5(0.5)
f <sub>8</sub>	56.065747	(42)	3.3(0.5)	2f <sub>5</sub>	38.225946	-	5.5(0.6)
V18				f <sub>10</sub>	38.961059	(33)	4.2(0.6)
f <sub>1</sub>	0.069108	(16)	10.8(0.6)	2f <sub>6</sub>	39.523246	-	75.2(0.6)
f <sub>2</sub>	1.398965	(31)	4.7(0.7)	f <sub>11</sub>	40.367636	(42)	3.0(0.5)
f <sub>3</sub>	1.647285	(38)	4.8(0.6)	f <sub>12</sub>	46.114884	(30)	4.6(0.5)
f <sub>4</sub>	2.623331	(44)	4.3(0.8)	f <sub>13</sub>	47.232920	(54)	2.6(0.5)
f <sub>5</sub>	20.542125	(50)	2.7(0.5)	f <sub>14</sub>	58.991013	(51)	2.6(0.5)
f <sub>6</sub>	23.564537	(14)	9.6(0.5)	3f <sub>6</sub>	59.284869	-	22.8(0.5)
V19				4f <sub>6</sub>	79.046492	-	11.3(0.5)
f <sub>1</sub>	0.643866	(49)	2.9(0.6)	5f <sub>6</sub>	98.808115	-	5.2(0.5)
f <sub>2</sub>	1.001649	(40)	5.8(0.5)				
f <sub>3</sub>	22.833647	(6)	21.1(0.5)				
f <sub>4</sub>	45.667295	-	2.8(0.5)				

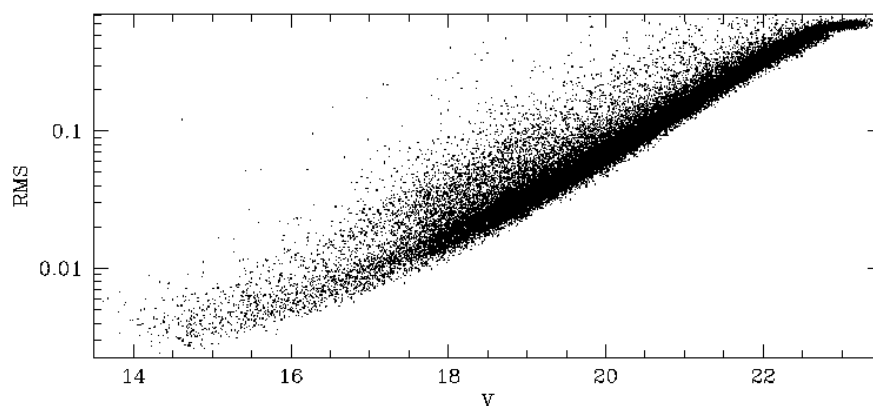


Figure 1: Standard deviation vs. average  $V$ -band magnitude for light curves of stars from the M10 field.

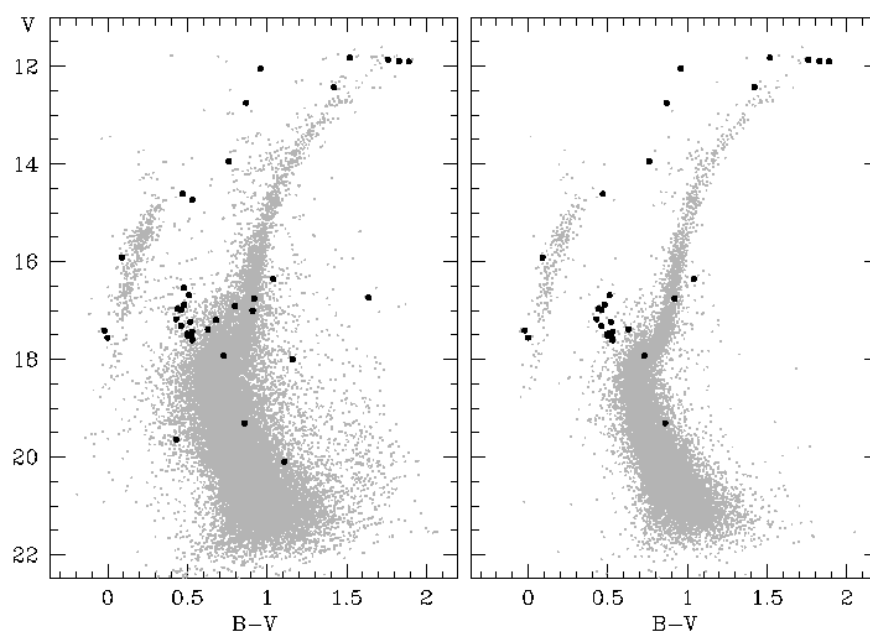


Figure 2: CMD for the observed field. Left: all stars for which proper motions were measured by N17. Black points mark all the variables detected within the present survey for which  $B$ -band magnitudes were available. Right: same as in the left panel, but for PM-members of the cluster only.



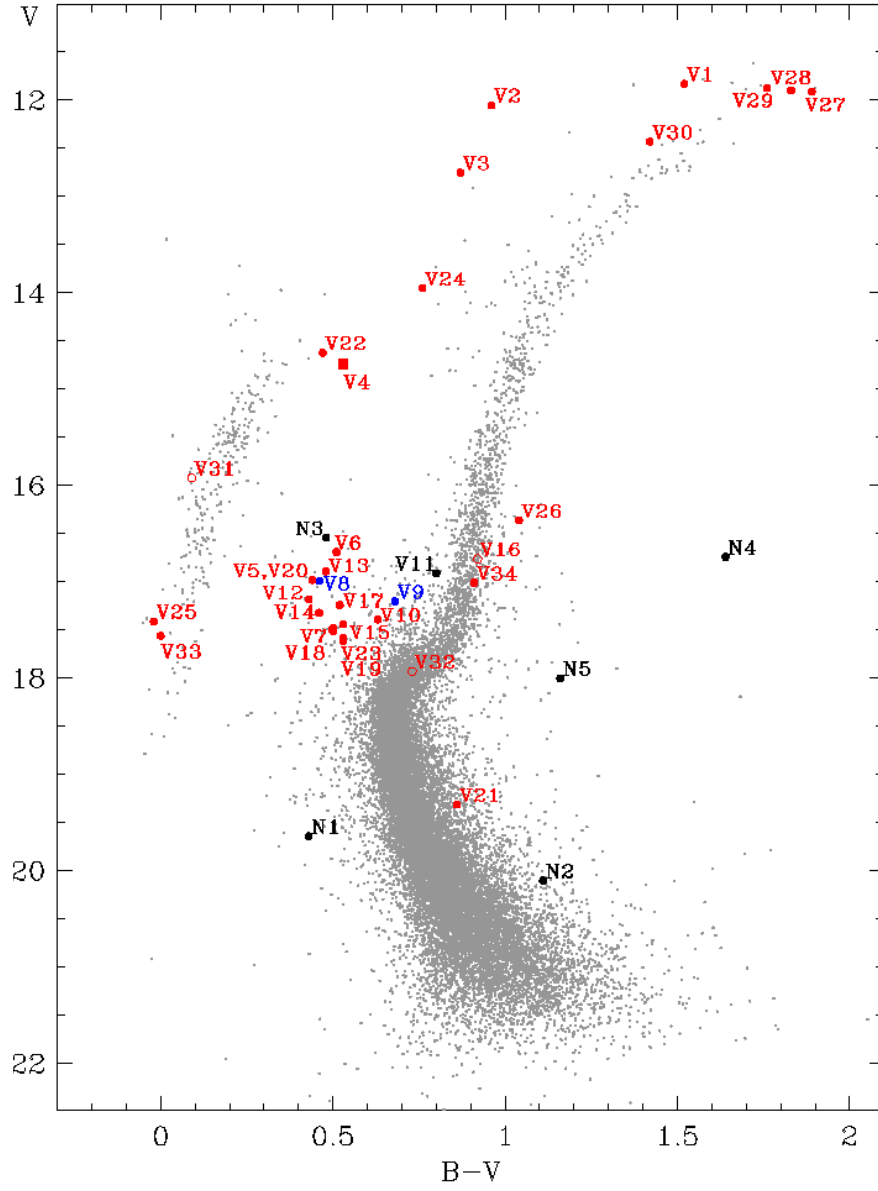


Figure 3: CMD for the observed field with locations of the variables identified within the present survey. Red: members of M10; blue: discrepant CASE and *Gaia* proper motions, black: field stars. Filled circles: confirmed variables; open circles: suspected variables; square: constant star listed as a likely RR Lyr-type pulsator by C17. The gray background stars are the same as in the right panel of Fig. 2.

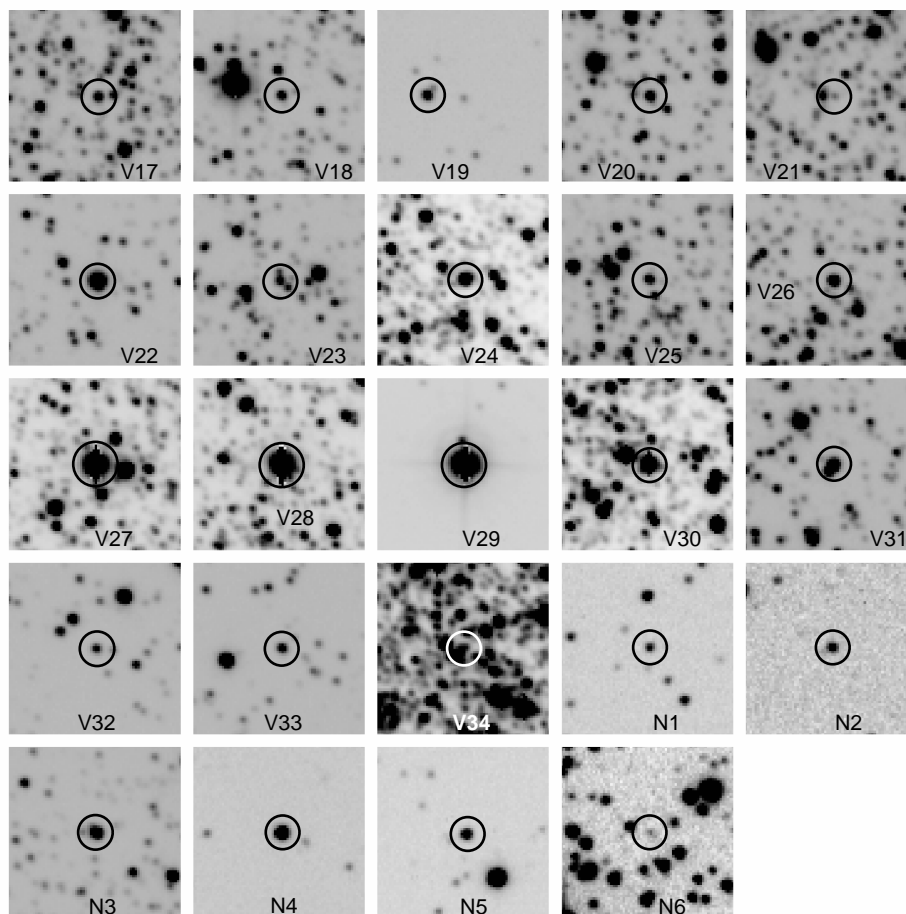


Figure 4: Finding charts for the new variables whose light curves are shown in Figs. 5 and 6. Each chart is 30'' on a side. North is up and East to the left.

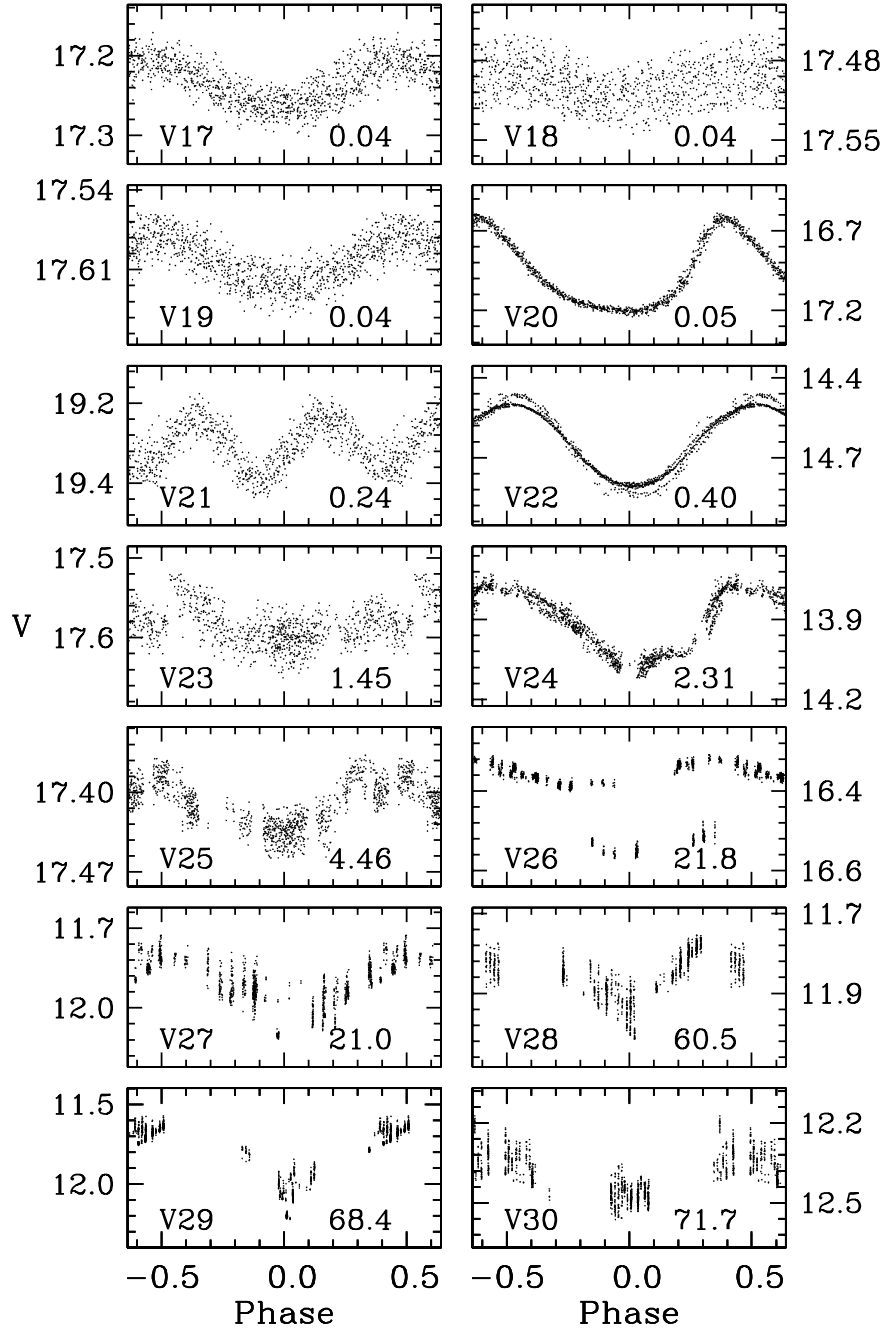


Figure 5: Phased V-band light curves for the newly discovered variables. Panel labels give star ID and period in days.

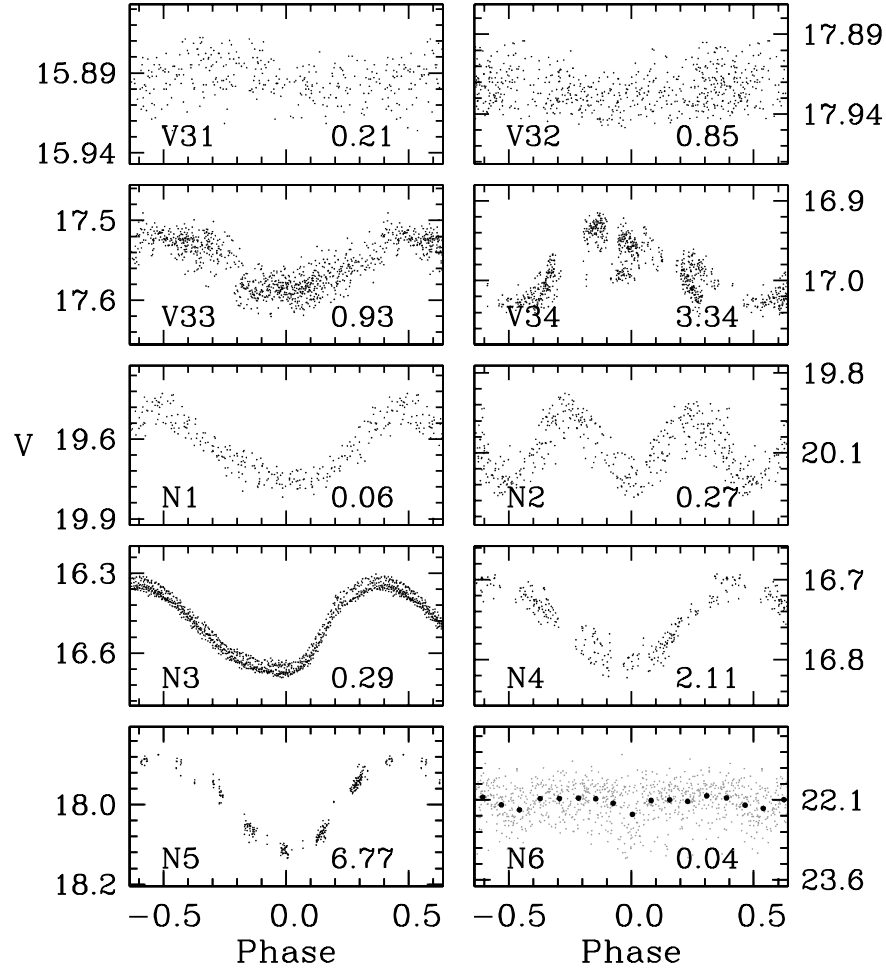


Figure 6: Continuation of Fig. 5 Phase-binned data for N6 are shown with heavy black points.

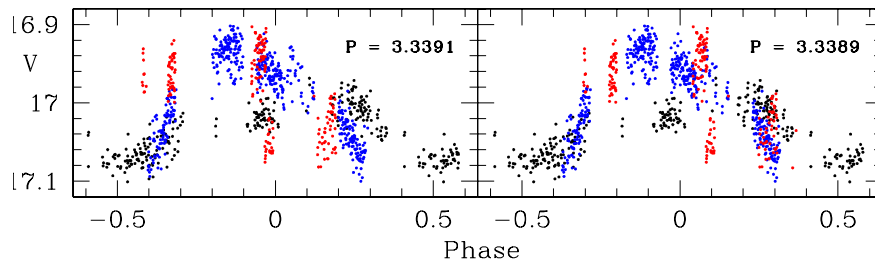


Figure 7: V-band light curve of V34 phased with  $P=3.3391$  d (left) and  $P=3.3389$  (right). Black, blue and red points: seasons 1998, 2002 and 2015, respectively.

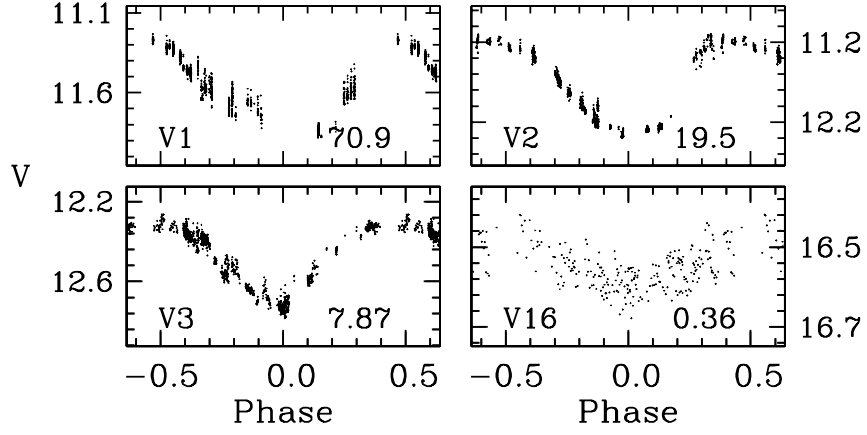


Figure 8: Phased V-band light curves for selected variables from the C17 catalog. Panel labels give star ID and period in days.

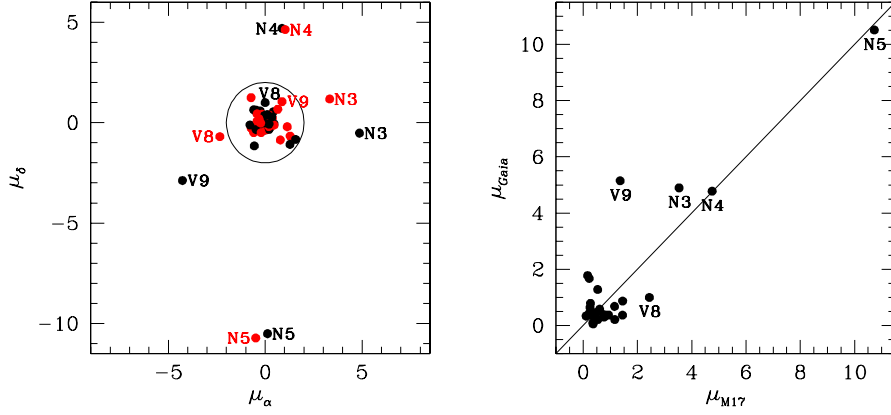


Figure 9: Left: *Gaia* proper motions in M10 frame (black) compared to those of N17 (red). Encircled are stars which, except V8 and V9, were used to derive the absolute proper motion of the cluster. Right: comparison of total proper motions  $\mu = \sqrt{\mu_\alpha^2 + \mu_\delta^2}$ . PM unit is  $\text{mas y}^{-1}$ .